LATVIAN JOURNAL OF PHYSICS AND TECHNICAL SCIENCES
2016, N 2

DOI: 10.1515/lpts-2016-0010

EXPERIMENTAL AND NUMERICAL ANALYSIS OF AIR FLOW, HEAT TRANSFER AND THERMAL COMFORT IN BUILDINGS WITH DIFFERENT HEATING SYSTEMS

A. Sabanskis, J. Virbulis

Laboratory for Mathematical Modelling of Technological and Environmental Processes, University of Latvia,
8 Zellu Str., Riga LV-1002, LATVIA

Monitoring of temperature, humidity and air flow velocity is performed in 5 experimental buildings with the inner size of 3x3x3 m^3 located in Riga, Latvia. The buildings are equipped with different heating systems, such as an air-air heat pump, air-water heat pump, capillary heating mat on the ceiling and electric heater. Numerical simulation of air flow and heat transfer by convection, conduction and radiation is carried out using OpenFOAM software and compared with experimental data. Results are analysed regarding the temperature and air flow distribution as well as thermal comfort.

Keywords**:** *experimental buildings, monitoring system, numerical simulation, OpenFOAM, thermal comfort.*

1. INTRODUCTION

Under growing demand for energy efficiency for building design and introduction of new alternative concepts for heating, the increased attention should be devoted to ensure the indoor environment quality.

In addition to the different types of radiant heating [1], the cost and energy efficient air-air heat pumps play an important role also in cold climate conditions [2]. Air-air heat pumps include controlled ventilation systems ensuring necessary air quality. Particular heating systems produce different flow and temperature distributions in the room, influencing both heating performance and thermal comfort.

A review of general and local thermal comfort models and elaborated standards in indoor ambiences is given in [3]. Popular standards such as ASHRAE 55-2004 and ISO 7730 are relatively compatible, in the present article the thermal comfort conditions are analysed as described in standard ISO 7730:2005 [4]. Standards suggest that thermal comfort can be expressed in terms of Predicted Mean Vote and Predicted Percentage Dissatisfied regarding the drought rate, vertical air temperature difference, warm or cool floor and radiant asymmetry.

Numerical simulations are often used for the investigation of heating and

cooling systems in buildings. Main advantages of simulations are the existence of calculated values of air flow and temperature in every point of the considered domain as well as the possibility to study the parameters already in the planning stage. However, experiments are utmost necessary to validate the models; therefore, experimental and numerical investigations are often combined [5], [6], [7].

In the present article, several radiant and air heating systems are investigated and compared regarding the flow pattern, temperature distribution, integral thermal behaviour and thermal comfort.

2. EXPERIMENTAL ENVIRONMENT

Five test stands with equal size and orientation in space (window on the south facade, doors on the north) have been built in the Botanical garden of the University of Latvia, Riga, Latvia [8]. They are denoted as AER, CER, EXP, LOG and PLY, which stand for the materials used for the walls – aerated concrete blocks, perforated ceramic blocks, perforated ceramic blocks filled with insulating granules, laminated beams and modular plywood panels, respectively. The walls are constructed to have the same thermal transmittance (U-value) of 0.16 W/m^{2}K. Internal size of each stand is 3x3x3 m^3. Internal components of the stands with the considered heating systems are shown in *Fig. 1*. The geometry of the system with a capillary heating mat on the ceiling is the same as for the air-water heat pump (*Fig. 1b*).

The following heating systems were used: air-air heat pump in LOG and AER, air-water heat pump in PLY, air-water heat pump with a capillary heating mat on the ceiling in EXP and electric heater in CER. An air-air heat pump was installed in all buildings and used for ventilation only in the PLY, EXP and CER stands. The main air circulation is between the air inlet and air feedback in the internal block of the air-air heat pump. Some amount of fresh air is mixed to this flow and the same amount of air is leaving through the ventilation outlet placed over the window.

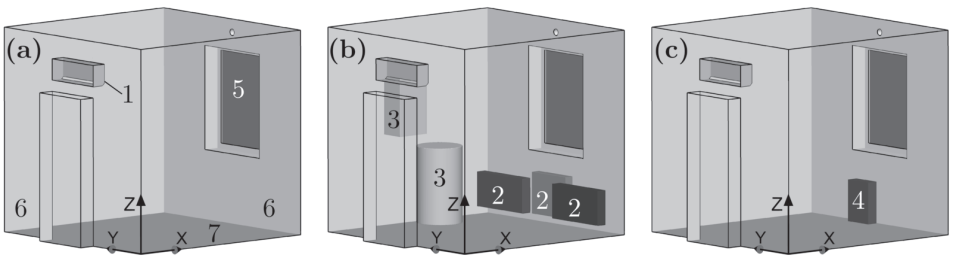

Fig. 1. Geometry of the systems with (a) air-air heat pump (1 – internal block), (b) air-water heat pump (2 – convectors; 3 – internal blocks) and (c) electric heater (4). Other denotations: 5 – window; 6 – walls; 7 – floor. Doors are located opposite the window.

3. MEASUREMENT SYSTEM

Identical sensors are installed in all test stands and are linked to the web-based data acquisition system for the automatic collection of data [9]. In the present study,

the temperature measurements in the middle of the room in 5 points at different vertical positions (0.1 m, 0.6 m, 1.1 m, 1.7 m from floor and 0.1 m from ceiling) are used for the comparison with the simulated temperature distribution. Repeatability of the used temperature sensors is ±0.1 °C, and the accuracy is ±0.3 °C [10].

4. NUMERICAL MODEL

For the numerical calculations of air flow and heat transfer, the modified calculation program chtMultiRegionSimpleFoam from the OpenFOAM version 2.3 open source code library [11] is used. Temperature was calculated in the air and solid domains (walls, ceiling, floor, window, doors).

The air flow is considered stationary and is described by the continuity and momentum equations. Air density ρ is calculated by the ideal gas law. The SST k-ω turbulence model with default model coefficients is used [11], [12], [13]. The no-slip condition has been applied at the solid walls. The velocity $\vec{U}$ at the ventilation outlet is specified according to the desired air exchange rate.

The enthalpy formulation is used for the calculations of energy transfer in the air and solid domains [11]. A constant outdoor temperature is applied at the external surfaces. Thermal radiation is calculated by the view factor model, which takes into account visibility of the surface elements, as well as their temperature and emissivity.

The thermal conductivities of solid domains were taken from [14] where the effective conductivity values were calculated to obtain the U-value of 0.16 W/m^{2}K. The following values of κ (in mW/(m·K)) were used: 91.8 for walls (EXP stand), 66.2 and 48.2 for the two-layered ceiling, 82.971 and 50.805 for the two-layered floor, 35.433 for the window, 62.532 for doors.

The balance of mass flow rate and heat fluxes has to be satisfied for the converged stationary solutions. The mass flow rate Q in kg/s through surface S is calculated by integrating the mass flux $\rho\vec{U}$.

There is one air inlet (denoted by "i") and two outlets (ventilation denoted by "v" and air feedback denoted by "f"). The mass conservation law reads $Q_i+Q_v+Q_f=0$, where the signs of the mass flow rates are $Q_i>0$, $Q_v<0$ and $Q_f<0$.

The conductive heat flux P_q through surface S is calculated using the temperature gradient. The net heat flux P_r radiated by surface S is computed by integrating the net radiation heat flux density. The convective heat flux P_c is calculated using 0°C as the reference temperature. The heater power is calculated as the sum of the conductive (P_q) and radiation (P_r) heat fluxes: $P_h=P_q+P_r$.

Since the temperature field inside the heaters is not considered, the surface temperature of the heaters is specified and the power is calculated during the post-processing stage. The used method allows describing cases with a heater turned off by setting $P_q=0$. In this case, $P_h=P_r$, which depends on the thermal conditions and in a general case does not vanish.

The power P_{aa} consumed by the air-air heat pump is calculated as follows:

$$P_{aa} = P_{c,i} + P_{c,v} + P_{c,\text{out}}, \qquad P_{c,\text{out}} = \int_S \rho\, c_p\, (T_{\text{out}} - T_0)\, \vec{U}\, d\vec{S},$$

where the convective heat fluxes P_c are calculated at the inlet and outlets, as defined previously. The signs are $P_{c,i} > 0$, $P_{c,v} < 0$ and $P_{c,\text{out}} < 0$. For the cases when the air-air heat pump is only used for ventilation, $P_{aa} = 0$ and the temperature at the inlet is calculated as follows: $T_i = -\left(P_{c,v} + P_{c,\text{out}}\right)/\left(c_p Q_i\right)$.

The mean radiant temperature used for the analysis of thermal comfort is calculated by the equation

$$\text{MRT} = \left(\sum_{i=1}^{N} F_{0i} T_i^4\right)^{1/4},$$

where F_{0i} is the diffuse view factor and N is the number of the radiating elements.

For the thermal comfort analysis, the difference between the MRT on the opposite sides of an imaginary plane element is calculated: $\Delta\text{MRT}_{\text{ud}}$ (up-down) in +z and –z direction, $\Delta\text{MRT}_{\text{fb}}$ in +x and –x direction, and $\Delta\text{MRT}_{\text{lr}}$ in +y and –y direction.

5. RESULTS AND DISCUSSION

5.1. Experiments

The previously measured air exchange rates in the test stands reported in [8] are in the range from 0.43 to 0.50 h^{-1}. It has also been verified that more than 90 % of the air exchange is due to air flow through the ventilation opening.

Since the simulations are stationary, the modelling results should be compared with experiments carried out under utmost steady conditions. To obtain such experimental results, louvers of the air-air heat pump were fixed in all test stands. The time-averaged temperatures in the middle of the stands at different vertical positions are shown in *Fig. 4*. Averaging was done on 2nd December 2014, over 9.2 h. During the experiment the temperature outside varied between -6°C and -8°C and solar radiation from cloudy sky changed between 0.5 W/m^2 in the night and up to 40 W/m^2 during the day, so the solar heat sources through the window were neglected.

5.2. Simulations

5.2.1. Summary of Considered Cases

In *Table 1*, the cases considered in simulations are summarised. The parameters are: T_i – temperature at inlet of air-air heat pump, U_i – inlet velocity, α_i – direction of inlet with respect to x axis ($\alpha_i = 0°$ corresponds to horizontal inflow, $\alpha_i = 90°$ – to inflow vertically downwards), P – heating power, T_{avg} – average temperature of the air, T_{floor} – average temperature of the floor. The temperature at the external walls of solid domains was set to -6°C and air exchange rate – to 0.45 h^{-1}. Cases aa1, el1, wa1 and cm1 correspond to the conditions in experiments and other cases study the effect

of inlet velocity and direction.

Table 1

Summary of the Modelled Cases

Case	Heating	T_i, °C	U_i, m/s	α_i, °	P, W	T_{avg}, °C	T_{floor}, °C
aa1	air-air	22.9	2.0	70	415	19.7	18.0
aa2	air-air	22.9	2.5	70	435	20.2	19.1
aa3	air-air	22.9	1.6	60	410	19.3	16.5
el1	electric	17.8	2.0	70	420	18.5	18.1
el2	electric	17.7	4.0	60	403	18.1	17.6
wa1	water-air	19.2	2.0	70	436	19.9	19.4
wa2	water-air	19.5	3.1	60	436	19.9	19.4
cm1	ceiling mat	15.4	3.4	60	403	15.4	15.2

5.2.2. Mesh Generation and Numerical Aspects

3D hexahedra-dominant finite volume meshes for all the configurations were created using the OpenFOAM mesh generator snappyHexMesh [11]. An example of mesh for the case with water-air heat pump in different cross-section planes of air domain is shown in *Fig. 2*. Thickness of cells at the solid walls is 10 mm, which increases by a factor of 1.15 until a bulk cell size of 40 mm is reached.

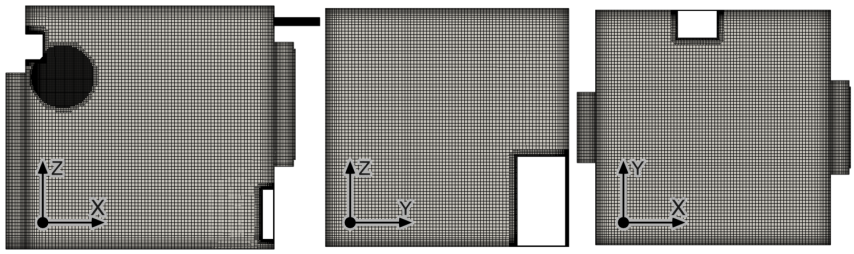

Fig. 2. Example of finite volume mesh for system with water-air heat pump, 2.0 million cells. The refinement region near the inlet of air-air heat pump appears black in the figure.

Additional mesh refinement is applied in the vicinity of the inlet of the air-air heat pump (black region in *Fig. 2*), with the cell size being 5 mm in the immediate vicinity of the heat pump, and 10 mm in the region of airflow from the inlet.

5.2.3. Air Flow and Temperature Distributions

Figure 3 shows the calculated velocity and temperature fields in the air for all considered cases. The white isolines of air flow velocity at U=0.2 m/s help distinguish between regions of high and low velocity. In all cases, contra-clockwise vortex with maximum velocity at inlet is generated. The shape of the vortex clearly correlates with the inflow angle and velocity. For a large angle (aa1, aa2, el1, wa1) the jet reaches the floor closer to the inlet side. The same is true for a larger velocity

(e.g. compare aa1 to aa2). Comparing the cases with the same inlet conditions (aa1, el1, wa1) the effect of the heating system can be seen as well.

Equal inlet temperature of 22.9 °C was used for the cases (aa1)–(aa3), while the inlet velocity and angle was varied. For a sufficiently large inlet velocity (aa1) and (aa2) hot air from the inlet reaches the floor, while in the case of reduced velocity (aa3) the buoyancy effects prevent this and the average floor temperature is lower by 1.5–2.6 °C. The different inlet velocities also affect the convective heat gain, and, as a result, the average air temperature. The high inflow rate (aa2) results in a better mixing of the air and reduces temperature variations.

In case of the capillary heating mat on the ceiling (cm1), the air temperature inside the room is the most homogeneous of all cases. The cases with the electric heater (el1 and el2) show strong upward flow which is affected by the inlet velocity – for small velocity (el1) air from the heater rises vertically upwards, while for twice as high velocity (el2) it deviates from the vertical direction. The temperature at the heater surfaces is 63.2 °C and 56.9 °C for el1 and el2, respectively.

The cases with the water-air heat pump (wa1) and (wa2) behave similarly as the cases with the electric heater – for the large inflow velocity the hot air is dragged along and a distinct vortex is formed. The temperature distributions in the room are more homogeneous than in the cases with electric heaters, the temperature at the heater surfaces is 33.7 °C and 31.9 °C for (wa1) and (wa2), respectively.

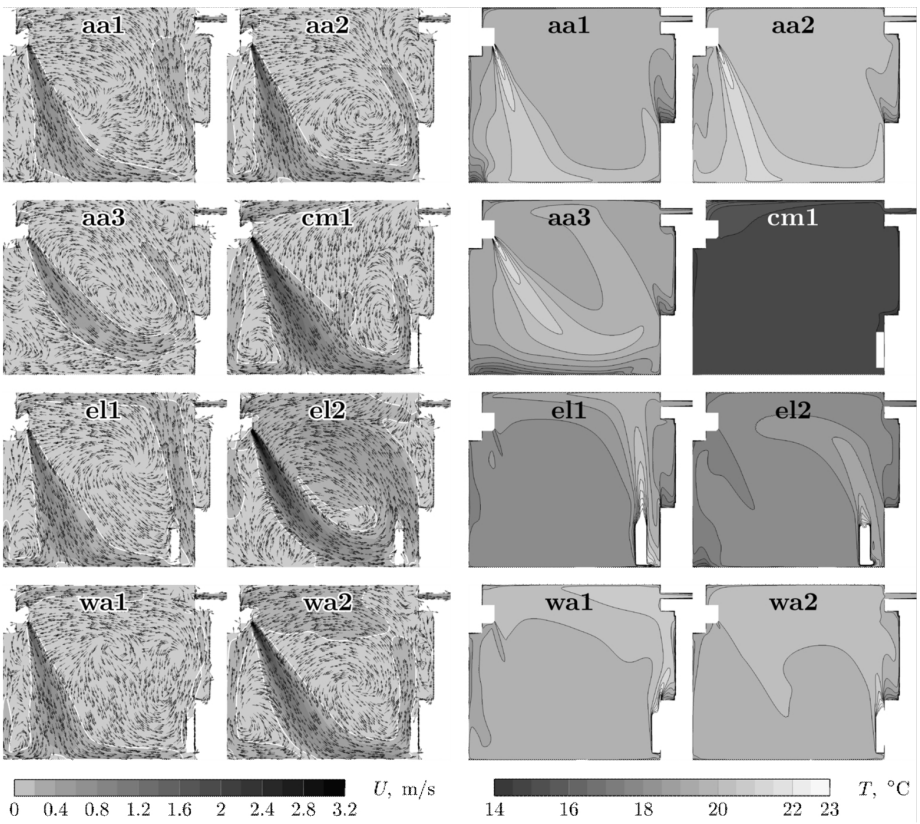

Fig. 3. Left: velocity field and isoline of U=0.2 "m/s" (white); right: temperature field (spacing between isolines is 0.5 °C).

5.2.4. Integral Thermal Analysis

Contrary to measurements in 5 points, the simulation results provide temperature and heat flux values in every point of the considered domain. Therefore, integral analysis can be done easily by averaging the calculated values over a volume or particular surfaces. The integral heat fluxes are summarised in *Table 2* where heat gains are positive and heat losses – negative. The calculated balance of all the heat fluxes SUM does not exceed 4 W or 1% in any case. The heating power of the air-air heat pump can be calculated as a sum of inflow and feedback heat fluxes.

The power used for heating is approximately the same for all cases in the range from 403 W (cm1) to 436 W (wa1). The mean air temperature varies between 15.4 °C (cm1) to 20.2 °C (aa2). However, there is no distinct correlation between the heater power and the air temperature. The air temperature depends more on the heating system, i.e. how efficient the heat is mixed into the air before leaving the room through construction elements and ventilation. The heat losses for different systems are compared using a kind of integral U-value calculated as the ratio of the heating power to the temperature difference (mean air temperature minus outdoor temperature) per m^2. It is 0.299–0.307 W/m^2K for the air-air system, 0.312 W/m^2K for the air-water heat pump system, 0.310–0.317 W/m^2K for the electrical heater and 0.349 W/m^2K for the ceiling mat. In the first case, the warm air is directly mixed into the convective vortex; in the case of the ceiling mat, mixing is smaller due to slow velocity at the ceiling and stratification of temperature.

Table 2

Integral Heat Fluxes in W

Case	Inflow	Ventilation	Feedback	Ceiling	Floor	Window	Doors	Walls	Heater	SUM
aa1	2203	-77	-1818	-39	-41	-27	-34	-171	-	-4
aa2	2753	-79	-2348	-40	-43	-27	-36	-177	-	3
aa3	1879	-75	-1499	-38	-39	-26	-33	-165	-	4
el1	1743	-77	-1768	-39	-41	-27	-34	-174	420	3
el2	3682	-70	-3707	-38	-41	-26	-33	-169	403	1
wa1	1871	-81	-1895	-41	-44	-28	-36	-184	436	-2
wa2	3168	-78	-3192	-41	-44	-28	-36	-183	436	2
cm1	2778	-62	-2806	-67	-37	-24	-30	-152	403	3

5.2.5. Comparison with Experiment

The comparison of the calculated vertical temperature distributions in the centre of the test stands with experiment is given in *Fig. 4*. Since the same heating conditions with the air-air heat pump were used in LOG and AER stands, the same simulation result is used in both comparisons. Despite the identical heating conditions in the AER and LOG stands, the measured temperature distribution slightly differs.

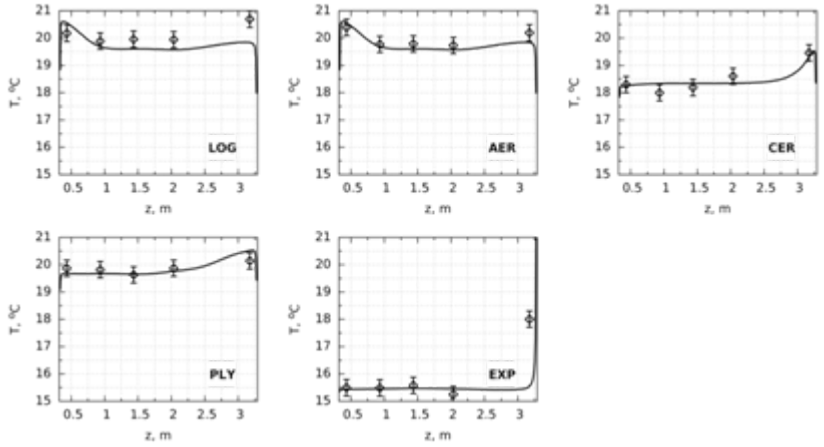

Fig. 4. Comparison of the calculated vertical temperature distributions in the centre of building (solid lines) with experiment (points).

In general, both the qualitative and quantitative tendencies are well-captured by the numerical simulations. The captured tendencies are higher temperature at the floor for the (aa1) case and higher temperatures at the ceiling for (wa1) and (el1) cases. The calculation results agree with the experiments within the measurement accuracy, except for the uppermost point in EXP. The capillary heating mat on the ceiling in EXP stand consists of thin capillaries and occupies a certain installation height, which is not considered in the modelling.

5.2.6. Radiant Temperature Asymmetry

As the numerical model considers the heat exchange by radiation, the radiant temperature, which is important for the thermal comfort, can be calculated. *Figure 5* shows the vertical distribution of the radiant temperature asymmetries ΔMRT_{ud} and ΔMRT_{fb} 0.5 m from the window. Only five cases are depicted since there are small differences between (aa1) and (aa2), (el1) and (el2) and between (wa1) and (wa2).

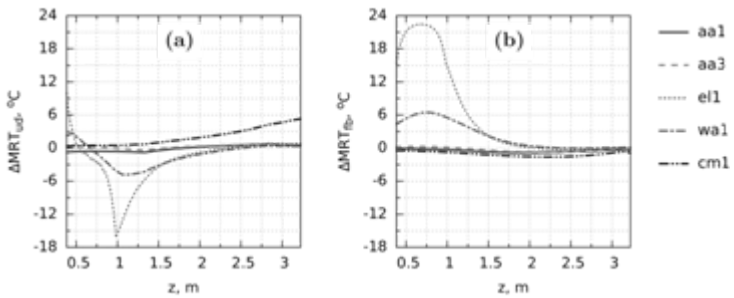

Fig. 5. Vertical distributions of radiant temperature asymmetry 0.5 m from the window (a) ΔMRT_{ud} between up and down (+z and –z); (b) ΔMRT_{fb} between front and back (+x and –x).

The inflow velocity for (aa1) is sufficiently strong to reach the floor and heat it, resulting in $\Delta MRT_{ud} < 0$ in the lower part of the room. For (aa3), the temperature of the ceiling is higher than that of the floor; therefore, $\Delta MRT_{ud} > 0$.

For the (el1) system, the distributions are strongly affected by the high-temperature heater. The maximum vertical asymmetry is observed at its upper z coordinate of 98.4 cm. Face to bottom asymmetry $\Delta MRT_{fb} > 0$ since the heater is located in the +x direction, and it reaches about 22 °C in the vicinity of the heater.

The qualitative behaviour of the (wa1) case is similar to (el1). The maximum of vertical asymmetry is observed at the upper z coordinate of the heater of 105 cm.

5.2.7. Thermal Comfort

The thermal comfort is analysed based on the standard ISO 7730:2005 [4]. For the highest category A thermal environment the restrictions are drought rate DR < 10 %, vertical air temperature difference Percentage Dissatisfied (PD) < 3 %, warm or cool floor PD < 10 %, and radiant asymmetry PD < 5 %. These values are recalculated to maximum allowable flow velocity and temperature difference using formulas from [4] under consideration of clothing and activity level.

For the local temperature of 23 °C, the condition for the draught rate DR < 10 % yields the maximum velocity of 0.18 m/s. Analysing the calculated velocity fields (see *Fig. 3*, isoline of 0.2 m/s), it is concluded that the inflow velocity of the air-air heat pump (or ventilation device) is sufficiently high and the thermal comfort conditions regarding the draught rate are not satisfied in small-size test stands.

The condition PD < 3 % for the vertical air temperature difference between the head and ankles corresponds to the maximum temperature difference of 2.7 °C or 6 temperature isolines in *Fig. 3*. All the considered cases except aa3 satisfy this comfort condition since the temperature differences do not exceed 1.5 °C.

The condition PD < 10 % for the warm or cool floor corresponds to the floor temperature in the range of 19.2–28.0 °C. By analysing the average floor temperatures in *Table 1*, it is concluded that this condition is satisfied only for the cases with the highest heating power – wa1 and wa2. The experimental target temperature of 20 °C was 2 °C lower than the optimum operative temperature of 22°C in A class buildings [4]. If the temperature is increased by 2 °C by increasing the heating power, the cold floor condition will not be satisfied only for cases (cm1) and (aa3).

The condition PD < 5 % for the radiant temperature asymmetry corresponds to the maximum radiant temperature asymmetry of 4.0 °C for warm ceiling and 25.8 °C for warm wall. For (el1), (el2) and (cm1) the condition for a warm ceiling is not satisfied.

6. CONCLUSIONS

It has been demonstrated that the numerical modelling is a valuable tool, which supplements experimental measurements and allows gaining more insight into heat and mass transfer and thermal comfort in rooms. The developed mathematical model has been validated by comparing the temperature distributions in the middle of the room for four different experimental setups, and rather good agreement with experiment is achieved.

The air-air heat pump system produces the highest mean air temperature per applied thermal heating power, followed by air-water heat pump, electrical heater and capillary ceiling mat.

The thermal comfort cannot be satisfied with respect to the draught rate if the air-air heat pump is used for ventilation in the considered small-size test stands. For the vertical air temperature difference between the head and ankles, the comfort conditions are satisfied when using air-air heat pump in ventilation mode together with any other heating system. The comfort regarding cool floor can be satisfied by increasing the heating power, but the air-air heat pump with slow inflow velocity and ceiling mat are unfavourable solutions. The discomfort of radiant temperature asymmetry is observed in case of capillary heating mat and close to the electric heater.

ACKNOWLEDGEMENTS

The present research has been supported by the European Social Fund; the project is implemented by the University of Latvia, No. 2013/0027/1DP/1.1.1.2.0/13/APIA/VIAA/007.

REFERENCES

1. Rhee, K.N., Kim, K.W. (2015). A 50 year review of basic and applied research in radiant heating and cooling systems for the built environment. *Building and Environment 91*, 166–190.
2. Hakkaki-Fard, A., Eslami-Nejad, P. Aidoun, Z., and Ouzzane, M. (2015). A techno-economic comparison of a direct expansion ground-source and an air-source heat pump system in Canadian cold climates. *Energy 87* (1), 49–59.
3. Garcia, J.A. (2010). A Review of General and Local Thermal Comfort Models for Controlling Indoor Ambiences. *Air Quality*, Ashok Kumar (Ed.), ISBN: 978-953-307-131-2, InTech.
4. ISO 7730:2005. (2005). *Ergonomics of the Thermal Environment – Analytical Determination and Interpretation of Thermal Comfort Using Calculation of the PMV and PPD Indices and Local Thermal Comfort Criteria.* Geneva, Switzerland: International Organization for Standardization.
5. Myhren, J.A., and Holmberg S. (2008). Flow patterns and thermal comfort in a room with panel, floor and wall heating. *Energy and Buildings 40* (4), 524–536.
6. Stamou, A., and Katsiris, I. (2006). Verification of a CFD model for indoor airflow and heat transfer. *Building and Environment 41* (9), 1171–1181.
7. Tiberiu C., Virgone, J., and Kuznik, F. (2009). Evaluation of thermal comfort using combined CFD and experimentation study in a test room equipped with a cooling ceiling. *Building and Environment 44* (8), 1740–1750.
8. Jakovics, A., Gendelis, S., Ratnieks, J., and Sakipova, S. (2014). Monitoring and Modelling of Energy Efficiency for Low Energy Testing Houses in Latvian Climate Conditions. *International Journal of Energy. 8*, 76–83.
9. Greitans, M., Grunde, U., Jakovics, A., and Gendelis, S. (2013). Web-based real-time data acquisition system as tool for energy efficiency monitoring. In: 21st Telecommunications Forum (TELFOR), 26–28 November 2013 (pp. 553–556). Belgrade, Serbia: IEEE.

10. Datasheet SHT7x Humidity and Temperature Sensor IC. (2015). Available at http://www.sensirion.com/fileadmin/user_upload/customers/sensirion/Dokumente/Humidity/Sensirion_Humidity_SHT7x_Datasheet_V5.pdf.
11. The Open Source CFD Toolbox OpenFOAM. (2015). Available at http://www.openfoam.org/
12. Langley Research Center Turbulence Modelling Resource. (2015). Available at http://turbmodels.larc.nasa.gov/sst.html.
13. Menter, F. R., Kuntz, M., and Langtry, R. (2003). Ten Years of Industrial Experience with the SST Turbulence Model. *Turbulence, Heat and Mass Transfer. 4*, 625–632.
14. Ratnieks, J., Jakovičs, A., and Gendelis, S. (2014). Mathematical modelling of airflow velocity and temperature fields for experimental test houses. In: Proceedings of the 10th Nordic Symposium on Building Physics, 15–19 June 2014, (pp. 871–878). Lund, Sweden.

GAISA PLŪSMAS, SILTUMA PĀRNESES UN TERMISKĀ KOMFORTA EKSPERIMENTĀLA UN SKAITLISKA ANALĪZE ĒKĀS AR DAŽĀDĀM APKURES SISTĒMĀM

A. Sabanskis, J. Virbulis

K o p s a v i l k u m s

Temperatūras, mitruma un gaisa plūsmas monitorings veikts 5 eksperimentālās ēkās ar iekšējiem izmēriem 3x3x3 m^3, kas atrodas Rīgā, Latvijā. Ēkas ir aprīkotas ar dažādām apkures sistēmām, tādām kā gaiss-gaiss siltumsūknis, gaiss-ūdens siltumsūknis, griestu kapilārais sildīšanas paklājs un elektriskais sildītājs. Gaisa plūsmas un siltuma pārneses konvekcijas, vadīšanas un starojuma ceļā skaitliska modelēšana veikta izmantojot OpenFOAM programmatūru un iegūtie rezultāti salīdzināti ar eksperimentāliem datiem. Rezultāti tiek analizēti attiecībā uz temperatūras un gaisa plūsmas sadalījumiem kā arī termisko komfortu.

28.07.2015.